

The remnant of a merger between two dwarf galaxies in Andromeda II

Nicola C. Amorisco¹, N. Wyn Evans², Glenn van de Ven³

¹*Dark Cosmology Centre, Niels Bohr Institute, University of Copenhagen, Juliane Maries Vej 30, DK-2100 Copenhagen, Denmark; amorisco@dark-cosmology.dk*

²*Institute of Astronomy, University of Cambridge, Madingley Road, Cambridge, CB3 0HA, UK*

³*Max Planck Institute for Astronomy, Königstuhl 17, 69117 Heidelberg, Germany*

Driven by gravity, massive structures like galaxies and clusters of galaxies are believed to grow continuously through hierarchical merging and accretion of smaller systems. Observational evidence of accretion events is provided by the coherent stellar streams crossing the outer haloes of massive galaxies, such as the Milky Way¹ or Andromeda². At similar mass-scales, around 10^{11} solar masses in stars, further observational evidence of merging activity is also ample^{3,4,5}. Mergers of lower-mass galaxies are expected within the hierarchical process of galaxy formation⁶, but have hitherto not been seen for galaxies with less than about 10^9 solar masses in stars^{7,8}. Here, we report the kinematic detection of a stellar stream in one of the satellite galaxies of Andromeda, the dwarf spheroidal galaxy Andromeda II, which has a mass of only 10^7 solar masses in stars⁹. The properties of the stream show that we are observing the remnant of a merger between two dwarf galaxies. This had a dramatic influence on the dynamics of the remnant, which is now rotating around its projected major axis¹⁰. The stellar stream in Andromeda II illustrates the scale-free character of the formation of galaxies, down to the lowest galactic mass scales.

Andromeda II (And II) is, in size, the second largest dwarf spheroidal galaxy known in the Local Group, with a half light radius¹¹ of about 1.2 kpc (second only to And XIX¹²). With a luminosity⁹ of $L_V = 9.4 \times 10^6 L_\odot$, it currently sits¹³ at a distance of 185 kpc from its host, and at an heliocentric distance of about 650 kpc. Among the satellites of M31, And II is one of the few for which a spectroscopic dataset of hundreds of stars is currently available. These observations, made using the Deep Imaging Multi-Object spectrograph (DEIMOS) on the Keck II telescope, revealed a strong and puzzling stellar rotation, so far unique among the dwarf spheroidal galaxies of the Local Group¹⁰. The results presented here are based on a re-analysis of the latter spectroscopic observations, kindly provided by N. Ho and M. Geha.

We assign reliable probabilities of membership to all spectroscopic targets, comprising more than 700 candidate red giant branch stars, by allowing for the presence of both foreground contaminants from the Milky Way and interlopers from the halo population of M31. Each of the three coexisting components (members, Milky Way halo contaminants, M31 halo contaminants)

are described by a distinct spatial and kinematical distribution, the parameters of which are measured through a maximum likelihood technique (see Methods). A Bayesian approach then allows us to estimate a probability of membership for each available star: we count 632 high probability members ($p > 0.85$; see Extended Data Fig. 1).

We then study the kinematical properties of And II also through a maximum likelihood method that fully takes into account the observational uncertainties on the line-of-sight velocity of each available giant star in the spectroscopic sample. We find that, within measurement errors (median value of 6.5 km s^{-1}), there are no significant deviations from the strong rotation field of And II. However, despite such a smooth mean velocity field and an otherwise flat velocity dispersion profile (see Extended Data Fig. 2), we identify a drop and asymmetries in the velocity dispersion field, especially in the circular annulus $0.9 \lesssim R/\text{kpc} \lesssim 1.7$.

In order to quantify the significance of these kinematic anomalies, we isolate a group of stars that is defined based only on its spatially connected location. Fig. 1a displays the giant stars identified as high-probability members in the spectroscopic dataset, superimposed on Subaru Prime Focus Camera image¹⁰ of And II. We select 134 stars over an annular, stream-like region covering an angle of 270° over the body of And II (blue points). These are compared to a control sample of 319 stars, comprising the remainder of the spectroscopic targets at comparable distances from the center of And II (red points). Although sharing a compatible rotational field, the stream-like region is found to be kinematically colder. Fig. 1b displays histograms for the line-of-sight velocity distribution of the available giant stars in both regions. Fig. 1c shows the normalized generalized histograms obtained after subtracting the mean stellar rotation field. Fig. 1d shows the probability distribution functions of the projected velocity dispersion σ . The blue dashed curves in Figs. 1b-d refer to the stream-like region, while the red curves are for the control sample. The probability that the velocities of the giant stars in the two described regions have been extracted from the same parent line-of-sight velocity distribution is negligible ($p < 3 \cdot 10^{-6}$). This shows that, together with the stellar population of And II, an additional kinematically colder component contributes a substantial fraction of the stars in the selected annulus.

Among the stars in the latter spatially connected stream-like region, we next use a Bayesian approach to identify those that are significantly better described by the properties of the control sample with a higher velocity dispersion, $\sigma = 9.3 \pm 0.6 \text{ km s}^{-1}$. These are likely And II stars, and we find 14 of such high probability contaminants ($p > 0.85$), which are displayed in Fig. 1a by open blue points. If we exclude these, the remaining 120 stars (filled blue dots) are characterized by a much colder velocity dispersion ($\sigma \lesssim 3 \text{ km s}^{-1}$), the probability distribution of which is shown by the blue full curve in Fig. 1d. We identify these stars with a stream that extends coherently for over 5 kpc in length, with an average thickness of 0.3 kpc.

The stellar stream contains at least 1/10 of the luminosity of And II, which allows us to put a safe lower bound to the total luminosity of the progenitor $L_V \gtrsim 10^6 L_\odot$ (see Methods). Furthermore, current photometric data do not suggest that the color spread of the red giant branch population of

the stream is dissimilar from the considerable spread of the And II population itself (see Extended Data Fig. 3). Together, these point to the progenitor of the stream being a dwarf galaxy with a total mass not too different from And II. A progenitor with such properties is not unexpected: recent kinematic studies of members of the Local Group have identified analogue dwarf galaxies with comparably low velocity dispersions around both the Milky Way¹⁴ and M31¹⁵.

The merger had a substantial influence on the dynamics and structure of the remnant. The colder stream and warmer control sample do not show statistically significant differences in the properties of their rotation, which may seem somewhat odd within the merger context. However, it is very likely that the orbital angular momentum between the merging dwarfs was much larger than the intrinsic net angular momentum of the stars in either of the dwarfs. Combined with a mass ratio expected to be not too far from unity, the torque exerted by the merging dwarf would have been substantial. This is most probably responsible for stars of the stream and control sample having the same rotation strength, as well as the puzzling orientation around the major axis – stellar rotation is nearly always around the minor axis, consistent with oblate axisymmetry (except for rotation around the major axis in some giant elliptical galaxies caused by triaxiality). At the same time, it is likely that more stars that once belonged to the stream’s progenitor are lurking in the spectroscopic dataset, but cannot be clearly disentangled from the stellar population of AndII because of their lower density contrast. The detection of such a stream also provides a natural explanation for the peculiar extended component of old stars⁹ with an effectively constant density out to a large radius of about 1.9 kpc seen in And II; the merger have puffed up the remnant’s stellar population. Although a particularly close tidal encounter¹⁶ with M31 may also have contributed to shaping the structure of And II, this remains very uncertain given the unknown proper motion of And II and consequent degeneracy in the modelling¹³.

We measure the line-of-sight velocity of the stream as well as its projected spatial position onto the body of And II and use this information to constrain its approximate orbit. As Fig. 2 shows, a simple model of an orbit in a spherical potential is capable of describing the available velocity and position measurements. Although it is not possible to infer the detailed properties of the gravitational potential of And II as the orbit is found to be almost circular, we are able to constrain the enclosed mass (stellar and dark matter) interior to the stream as follows: $M(< 1.5\text{kpc}) = 2.5_{-1.1}^{+3.1} \times 10^8 M_{\odot}$. This implies a mass-to-light ratio of $45_{-20}^{+60} M_{\odot}/L_{\odot,V}$, which is typical of dwarf spheroidal galaxies^{17,18}.

Even with a characteristic orbital velocity for the stream, dating the epoch of the And II merger remains challenging. The survival of cold kinematic clumps is strongly dependent on the properties of the gravitational potential in which they orbit^{19,20}. Nevertheless, the And II stream seems to lie on a nearly circular orbit and never passes close to the central regions of the galaxy, which allows it to retain coherence for a very long time. At the same time, dynamical friction can drag two mutually orbiting dwarf galaxies closer, causing a merger in just a fraction of the Hubble time. We estimate this process requires $\gtrsim 3$ Gyr, which provides us with an approximate lower limit to associate with the merger of the And II system.

Streams of disrupted and engulfed galaxies are abundant in the halo of the Milky Way, as memorably shown in the Sloan Digital Sky Survey’s ‘Field of Streams’¹ and by the disrupting Sagittarius galaxy²¹. However, the frequency and role of accretion onto low-mass galaxies, and in particular of dwarf-dwarf mergers, remains unclear, given the extremely limited observational evidence. Stellar over densities similar to shells have been discovered in the Fornax dwarf spheroidal galaxy²², suggestive of a late merger origin²³. Irregular isophotes^{24,25} and a kinematically cold spot¹⁹ indicate that Ursa Minor has suffered recent disturbance, most probably the accretion of a lower mass stellar system in the form of a stellar cluster. In this respect, And II represents a compelling case of a dwarf-dwarf merger.

Mergers between low-mass galaxies are predicted within the hierarchical framework of galaxy formation, but they are rare at present times. This is particularly true for dwarf satellite galaxies: after accretion onto their host, in this case M31, the cross-section for encounters between previously unrelated dwarf galaxies is very low^{26,27}, implying that subsequent merging activity is essentially limited to galaxies that were closely associated before infall. This makes the discovery of a tidal stream, originating from the engulfment of one dwarf satellite by another, particularly remarkable. As for merger events preceding infall, it is estimated⁶ that one in two dark matter haloes with a virial mass of $10^{10} M_{\odot}$ have experienced a major merger (mass ratio $\gtrsim 1/3$) between redshift 4 and 1, but data to confirm these figures are exceedingly scarce.

And II provides direct evidence for the importance of mergers even for the smallest and least luminous of galaxies. Just as for the largest giant ellipticals, merging and accretion were dominant processes in the formation of the dwarf galaxies we see today.

References

1. Belokurov, V., Zucker, D., Evans N. W., et al. The Field of Streams: Sagittarius and its Siblings. *Astrophys. J.* 642, L137-141 (2006).
2. Ibata, R., Irwin, M., Lewis, G., Ferguson, A., Tanvir, N. A Giant Stream of Metal-rich stars in the Halo of the Galaxy M31. *Nature* 412, 49-52 (2001).
3. Martínez-Delgado, D., Peñarrubia, J., Gabany, R.J., et al. The Ghost of a Dwarf Galaxy: Fossils of the Hierarchical Formation of a Nearby Spiral Galaxy NGC 5907, *Astrophys. J.* 689, 184-193 (2008).
4. Chonis, Taylor S.; Martínez-Delgado, David; Gabany, R.J. et al. A Petal of the Sunflower: Photometry of the Stellar Tidal Stream in the Halo of Messier 63 (NGC 5055), *Astron. J.* 142, 166-181 (2011).
5. Martínez-Delgado, D., Pohlen, M., Gabany, R. J., et al. Discovery of a Giant Stellar Tidal Stream around the Disk Galaxy NGC 4013. *Astrophys. J.* 692, 955-963 (2009).
6. Fakhouri, O., Ma, C.-P., Boylan-Kolchin, M. The Merger Rates and Mass Assembly Histories of Dark Matter Haloes in the two Millennium Simulations., *Mon. Not. R. Astron. Soc.* 406, 2267-2278 (2010).
7. Rich, R. M., et al. A tidally distorted dwarf galaxy near NGC 4449. *Nature* 482, 192-194 (2012).

8. Martínez-Delgado, D., et al. Dwarfs gobbling dwarfs: a stellar tidal stream around NGC 4449 and hierarchical galaxy formation on small scales. *Astrophys. J.* 748, L24 (2012).
9. McConnachie, A. W., Arimoto, N., Irwin, M. J. Deconstructing Galaxies: a Suprime-Cam survey of Andromeda II. *Mon. Not. R. Astron. Soc.* 379, 379-392 (2007).
10. Ho, N., Geha, M., Munoz, R. R., et al. Stellar Kinematics of the Andromeda II Dwarf Spheroidal Galaxy. *Astrophys. J.* 758, 124-136 (2012).
11. McConnachie, A. W., Irwin, M. J. Structural Properties of the M31 Dwarf Spheroidal Galaxies, *Mon. Not. R. Astron. Soc.* 365, 1263-1276 (2006).
12. McConnachie, A.W.; Huxor, A.; Martin, N.F. et al. A Trio of New Local Group Galaxies with Extreme Properties *Astrophys. J.* 688, 1009-1020, (2008).
13. Watkins, L. L., Evans, N. W., van der Ven, G. A Census of Orbital Properties of the M31 Satellites. *Mon. Not. R. Astron. Soc.* 430, 971-985 (2013).
14. Koposov, S. E., Gilmore, G.; Walker, M. G., et al. Accurate Stellar Kinematics at Faint Magnitudes: Application to the Botes I Dwarf Spheroidal Galaxy. *Astrophys. J.* 736, 146 (2011).
15. Collins, M. L. M., Chapman, S. C., Rich, R. M., et al. A Kinematic Study of the Andromeda Dwarf Spheroidal System. *Astrophys. J.* 768, 172 (2013).
16. Shaya, E. J., Tully, R. B. The formation of Local Group planes of galaxies. *Mon. Not. R. Astron. Soc.* 436, 2096-2119 (2013).
17. Walker, M. Dark Matter in the Galactic Dwarf Spheroidal Satellites in ‘Planets, Stars and Stellar Systems’ Vol. 5, Oswalt, T.D., Gilmore, G., Springer (2013)
18. Amorisco, N. C., Evans, N. W. Phase-space models of the dwarf spheroidals. *Mon. Not. R. Astron. Soc.* 411, 2118-2136 (2011).
19. Kleyna, J. Wilkinson, M. I., Gilmore, G., Evans, N. W. A Dynamical Fossil in the Ursa Minor Dwarf Spheroidal. *Astrophys. J.* 588, L21-24 (2003).
20. Sánchez-Salcedo, F. J., Lora, V., The survival of dynamical fossils in dwarf spheroidal galaxies in conventional and modified dynamics. *Mon. Not. R. Astron. Soc.* 407, 1135-1147 (2010).
21. Belokurov, V. Koposov, S., Evans, N. W., et al. Precession of the Sagittarius stream. *Mon. Not. R. Astron. Soc.* 437, 116-131 (2014).
22. Coleman, M., Da Costa, G. S., Bland-Hawthorn, J., et al. Shell Structure in the Fornax Dwarf Spheroidal. *Astron. J.* 127, 832-839 (2004).
23. Amorisco, N. C., Evans, N. W., A Troublesome Past: Chemodynamics of the Fornax Dwarf Spheroidal, *Astrophys. J.* 756, L2 (2012).
24. Irwin, M., Hatzidimitriou, D., Structural parameters for the Galactic dwarf spheroidals. *Mon. Not. R. Astron. Soc.* 277, 1354-1378 (1995).
25. Palma, C., Majewski, S. R., Siegel, M. H., et al., Exploring Halo Substructure with Giant Stars. IV. The Extended Structure of the Ursa Minor Dwarf Spheroidal Galaxy. *Astron. J.* 125, 1352-1372 (2003).
26. Tremaine, S., ‘Galaxy Mergers’ in ‘Structure and Evolution of Normal Galaxies’ (eds S.M. Fall, D. Lynden-Bell) pgg. 67-84, Cambridge University Press (1981).
27. De Rijcke, S.; Dejonghe, H.; Zeilinger, W. W.; Hau, G. K. T. Dwarf elliptical galaxies with

kinematically decoupled cores, *Astron. Astrophys.* 426, 53-63 (2004).

Acknowledgments. The authors are glad to thank Mike Irwin for discussions on the photometric properties of And II. The Dark Cosmology Centre (DARK) is founded by the Danish National Research Foundation (DNRF). This work was partially supported by Sonderforschungsbereich SFB 881 “The Milky Way System” (subproject A7) of the German Research Foundation (DFG).

Author contributions. NCA performed the candidate selection using methods originally developed with NWE, and the subsequent kinematic extraction together with GvdV. NCA, NWE and GvdV suggested and elaborated the stream model to explain the data. The paper was written by NCA, with contributions from the other two authors.

Corresponding author. Nicola C. Amorisco amorisco@dark-cosmology.dk

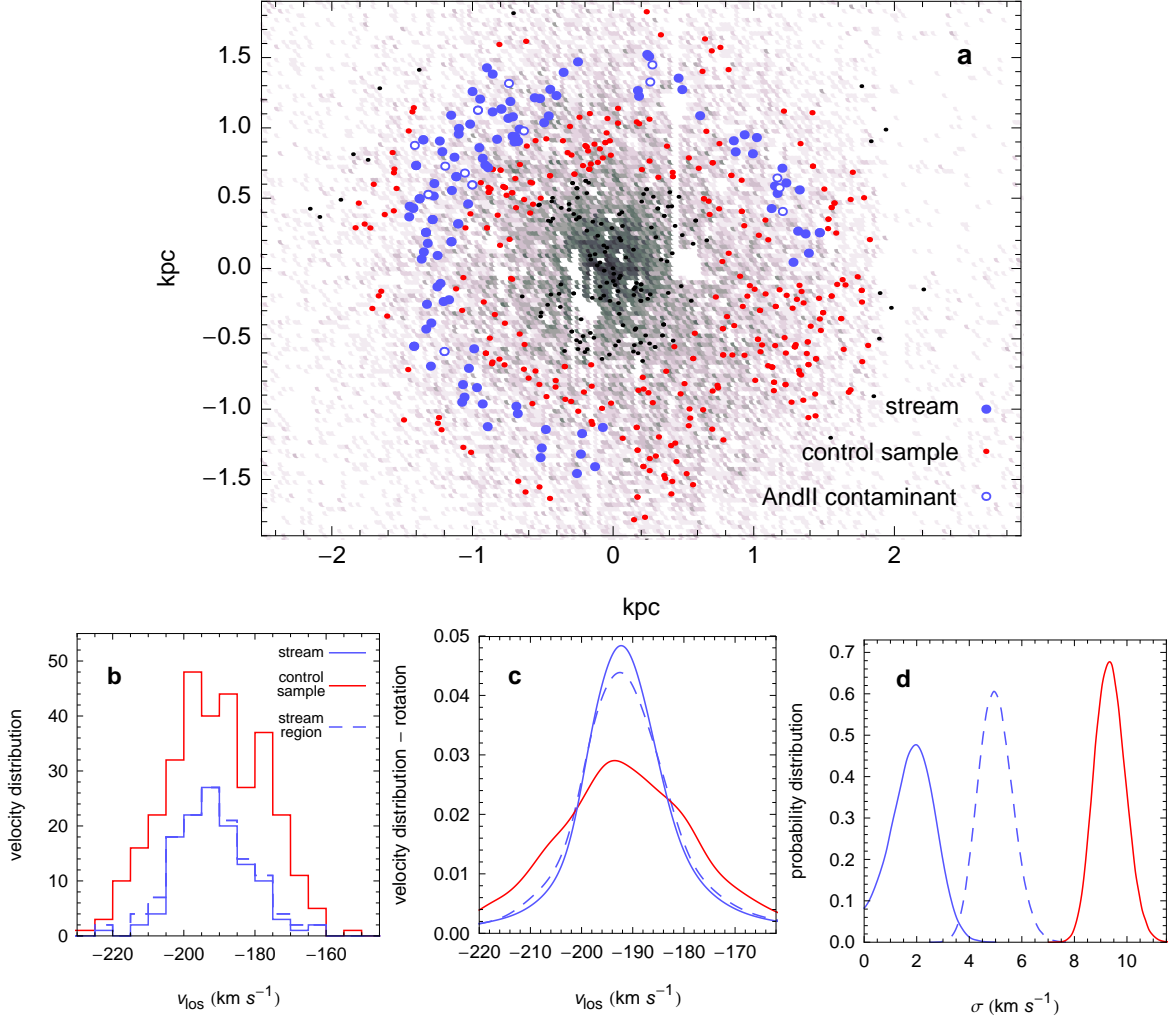


Figure 1 | Kinematic detection of a stream in And II. The targets in the circular annulus $0.7 < R/\text{kpc} < 1.9$ are divided into a kinematically cold and a warm component, panel **a**. The 134 stars in the connected stream-like region (blue points) yield the blue-dashed line-of-sight velocity distributions in panels **b** and **c** (respectively before and after normalisation, subtraction of the mean stellar rotation field and convolution with the individual measurement uncertainties), and the blue-dashed probability distribution for the projected velocity dispersion σ in panel **d**. Red distributions are associated with the kinematically warmer control sample, comprising the remaining 319 spectroscopic targets (red points). The 14 blue open points isolate stars which are more likely to belong to the main body of And II rather than to the stream itself. When they are subtracted from the sample of stream stars, the internal velocity dispersion of the stream is reduced further, leading to the blue full distributions.

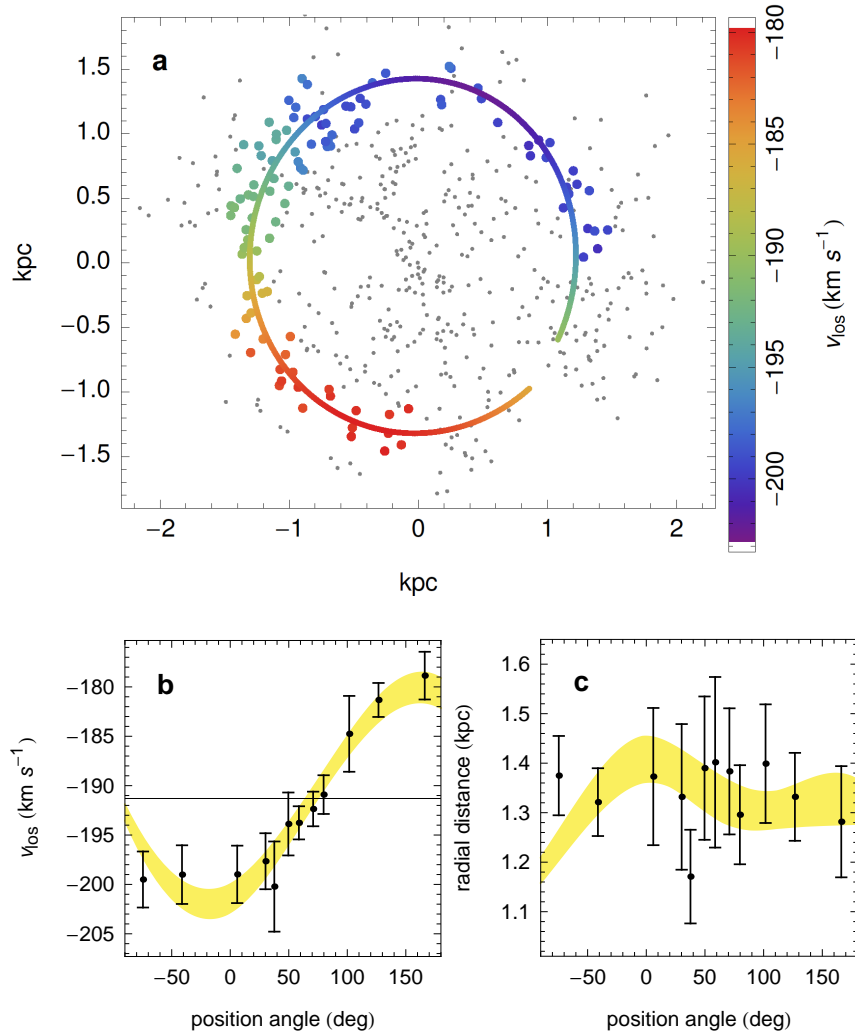


Figure 2 | The stream reproduced by an orbit in a spherical potential. The line-of-sight velocity (panel **b**) and distance from the centre of Andromeda II (panel **c**) of the stars belonging to the stream are reproduced by a simple model of an orbit in a spherical potential. Panel **a** displays the spectroscopic targets belonging to the stream, color-coded using a smoothed velocity field for comparison with the best-fitting orbit. Panels **b** and **c** show a direct comparison between the observables (each datapoint has been obtained by a subsets of 10 stream stars, error bars are s.d.) and the corresponding 68% confidence region obtained from the model.

Methods

I – Membership Selection.

In order to address the kinematical properties of And II, we need to separate the spectroscopic targets that belong to the red giant branch population of the dwarf galaxy from any contaminants. Contamination has two different origins: dwarf stars in the foreground belonging to the Milky Way and interlopers from the stellar halo of Andromeda. To reliably disentangle these three distinct components, we model the spectroscopic dataset as a superposition of multiple independent stellar populations, within the framework of a maximum likelihood technique^{23,28}:

$$L(\vec{\Theta}) = \prod_j \sum_i f_i P^{\text{sp}}(\vec{X}_j; \vec{\Theta}_i^{\text{sp}}) P^{\text{kin}}(v_j; \vec{\Theta}_i^{\text{kin}}). \quad (1)$$

The index j runs over the spectroscopic targets, while i indicates the three populations of the model, each containing a fraction of stars f_i , with the constraint $\sum_i f_i = 1$. The probability function P_i^{sp} , parametrized by the set of parameters $\vec{\Theta}_i^{\text{sp}}$, describes the spatial distribution of the members of the component i on the plane of the sky. Given the limited angular size of And II, we can adopt a constant surface density distribution for both populations of contaminants, while a Plummer density profile with elliptical isophotes is used to describe the population of And II itself. Analogously, the three components have different probability distributions for their kinematics, which are described by the function P^{kin} and the parameters $\vec{\Theta}_i^{\text{kin}}$. Given the significant separation of the contaminants from And II in terms of systematic velocity¹⁰, we can describe both the Milky Way and the Andromeda halo population with a simple Gaussian line-of-sight velocity distribution. The observational uncertainty on the measurement of the line-of-sight velocity of each single spectroscopic target, δ_j , is fully included in the analysis by formal convolution; hence, for the contaminants, we have:

$$P_{\text{cont}}^{\text{kin}}(v_j; v_i^{\text{sys}}, \sigma_i) = \frac{1}{\sqrt{2\pi(\sigma_i^2 + \delta_j^2)}} \exp\left[-\frac{1}{2} \frac{(v_j - v_i^{\text{sys}})^2}{\sigma_i^2 + \delta_j^2}\right], \quad (2)$$

where Milky Way and Andromeda contaminants have their own systematic velocity v_i^{sys} and intrinsic velocity dispersion σ_i . The velocity distribution of And II is also normally distributed, but has a rotating mean velocity field:

$$P_{\text{AndII}}^{\text{kin}}(v_j; v^{\text{sys}}, \vec{\Omega}, \sigma) = \frac{1}{\sqrt{2\pi(\sigma^2 + \delta_j^2)}} \exp\left[-\frac{1}{2} \frac{(v_j - v^{\text{sys}} - \vec{\Omega} \cdot \vec{X}_j)^2}{\sigma^2 + \delta_j^2}\right]. \quad (3)$$

The parameter space is explored by means of a suite of Monte Carlo chains, constructed using the Metropolis-Hastings algorithm²⁹. Once the best-fitting model is identified, for example as described by the set of parameters $\vec{\Theta}^{\text{bf}}$, a Bayesian approach allows us to estimate, for each spectroscopic target j , the probability of that individual star belonging to the population i :

$$p_j^i = \frac{f_i P^{\text{sp}}(\vec{X}_j; \vec{\Theta}_i^{\text{bf,sp}}) P^{\text{kin}}(v_j; \vec{\Theta}_i^{\text{bf,kin}})}{\sum_k f_k P^{\text{sp}}(\vec{X}_j; \vec{\Theta}_k^{\text{bf,sp}}) P^{\text{kin}}(v_j; \vec{\Theta}_k^{\text{bf,kin}})}. \quad (4)$$

Extended Data Fig. 1 shows the distribution of all spectroscopic targets in the plane (v_{los}, R) , where R is the projected radial distance from the centre of And II. Color-coding of each target is set by its probability of membership to And II: the combination of spatial position and kinematical information is capable of efficiently selecting the members of And II. As a further check, we also exclude a few targets that appear as fortuitous ‘kinematic members’, but whose membership to And II is questioned¹⁰ either by their colour ($V - I > 2.5$) or by the strength of the Na I line ($EW_{\text{Na I}} > 4$), which indicate that these may in fact be dwarf foreground stars from the Milky Way halo. As a result, we identify 632 giant stars belonging to And II with high probability ($p > 0.85$).

II – Kinematic extraction.

Despite significant observational effort and use of the DEIMOS spectrograph on Keck, the heliocentric distance of And II, $D \approx 650$ kpc, is so great that uncertainties on the measurement of the line-of-sight velocity of each target are significantly higher than figures achieved for the closer Milky Way dwarf satellites ($\delta_v \approx 2 \text{ kms}^{-1}$). In particular, with a median of about $\delta_v \approx 6.5 \text{ kms}^{-1}$, measurement errors are comparable in magnitude to the kinematical spread due to the intrinsic velocity dispersion of the dwarf, which implies that appropriate treatment of these uncertainties is crucial.

For this reason, we extract the kinematic properties of And II by fully taking into account all measurement errors, individually for each spectroscopic target. First, we adopt the line-of-sight velocity distribution of Equation 3 to infer the intrinsic velocity dispersion σ in circular annuli as displayed in Extended Data Fig. 2. The resulting σ profile is similarly flat as typically observed in dwarf spheroidal galaxies, except for a significant dip around $R \simeq 1.3$ kpc, independent of the precise choice of the circular annuli.

Next, we applied the same approach to stars in the circular annulus $0.9 \lesssim R/\text{kpc} \lesssim 1.7$, but now allowing for two spatially connected components with a different intrinsic velocity dispersion σ . This results in the identification of the stream-like region indicated by blue circles in panel **a** of Fig. 1 in the Letter. The convolution of the intrinsic line-of-sight velocity distribution with the assumed normally distributed error function of each target is illustrated in panel **c** of Fig. 1, which displays normalised generalised histograms for the velocity distributions of both stream and control sample. Only by explicitly including each measurement error individually it is then possible to infer the probability distributions of the intrinsic dispersion for stream and control sample, as shown in panel **d** of Fig. 1. Well over 10^5 draws in a suite of Monte Carlo chains have been used in order to accurately sample the tails of these σ distributions. This technique also ensures that these σ distributions are properly marginalised against uncertainties of all other parameters of the model.

III – Stream luminosity and progenitor.

Our kinematical analysis identifies $N_{\text{str}} = 120$ red giant stars as high probability members of the kinematically cold stream, in a pool of $N_{\text{mem}} = 632$ members of AndII. Although indicative of the significant luminosity of this structure, it is not entirely correct to simply use the ratio $N_{\text{str}}/N_{\text{mem}}$

to derive an estimate of the luminosity of the stream itself. This is because the stream covers a limited area over the body of And II and the spectroscopic coverage is neither uniform over the body of the dwarf nor proportional to its surface brightness profile.

We can instead obtain more accurate insight into the luminosity of the stream by restricting ourselves to the projected region it covers. This has been identified in Fig. 1a as an approximately annular region, centred around $R \approx 1.35$ kpc and covering an angle of $\approx 270^\circ$. By using the detailed surface density profile⁹ of And II, obtained by using deep Subaru Suprime-Cam data, we calculate that such projected area contains a fraction of $\approx 15\%$ of the total luminosity of the dwarf. In turn, we only find 14 high probability contaminants in this region, i.e. stars that are significantly more likely to belong to the And II population rather than to the kinematically cold stream. This implies a luminosity estimate for the stream of

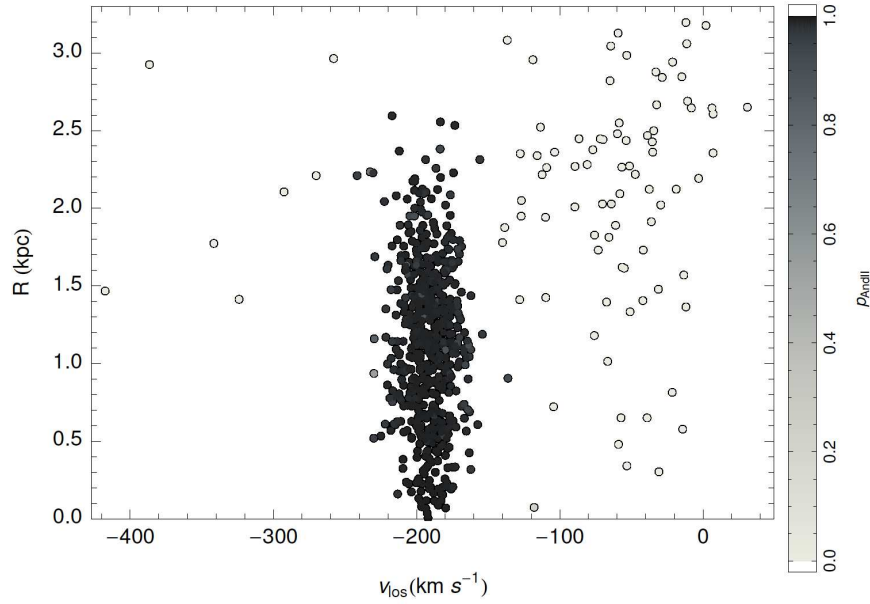
$$L_{V,\text{str}} \approx 0.15 \times \frac{120}{134} \times L_{V,\text{AndII}} \approx 0.13 \times L_{V,\text{AndII}} \approx 1.3 \times 10^6 L_\odot \quad (5)$$

It is worth mentioning that, based on kinematical data alone, we are inevitably only capable of identifying those parts of the stream which have a sufficiently high density contrast against the And II population, and whose kinematics in the stream’s progenitor were cold enough to stand out against the average current properties of And II. In particular, as a result of the merger, it is plausible that any stellar components that were originally more diffuse in the stream’s progenitor are now dispersed in And II, eluding a purely kinematical detection. This implies that the above 13% should be regarded as a lower limit for the luminosity of the progenitor itself.

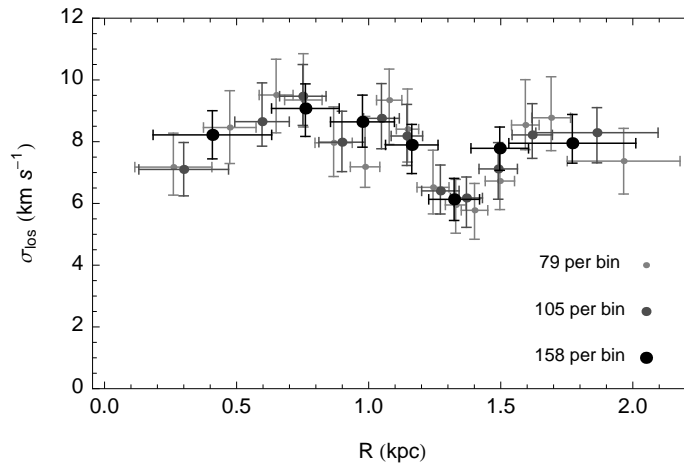
Whereas the resulting luminosity already makes a stellar cluster origin unlikely, this can be excluded further by considering the properties of the distribution of the stream’s members in the Colour Magnitude Diagram (CMD). Extended Data Fig. 3 follows the same stream versus control sample labeling as in panel **a** of Fig. 1 in the Letter to allow for the comparison of the properties of the stream’s member stars with the And II population. We find that this data suggest little difference in the distribution of such two populations in the CMD, highlighting that the stream also has a significant color spread.

Methods References.

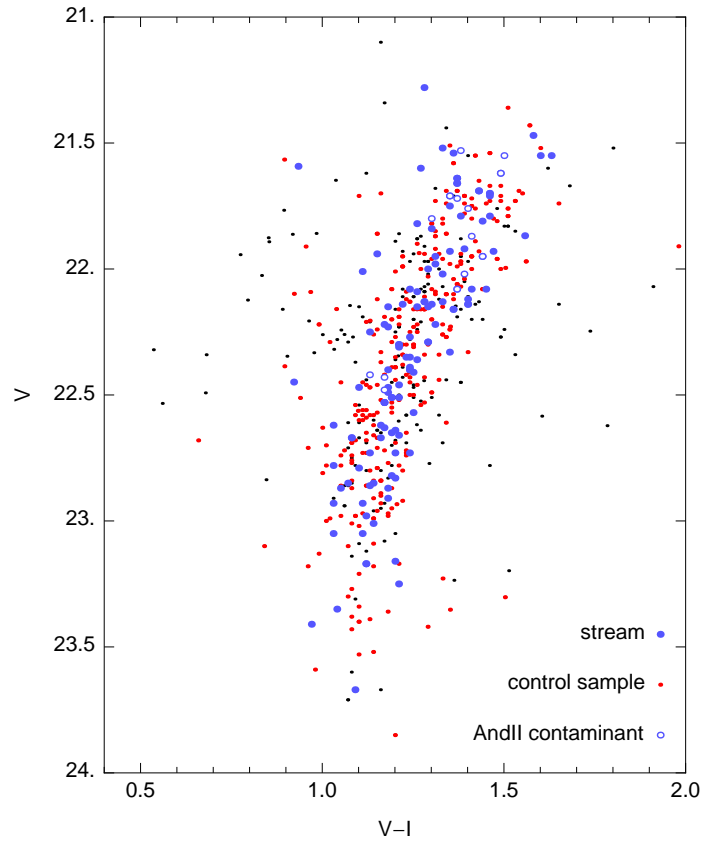
28. Walker, M. G., & Peñarrubia, J. A Method for Measuring (Slopes of) the Mass Profiles of Dwarf Spheroidal Galaxies. *Astrophys. J.* 742, 20 (2011).
29. Metropolis, N., Rosenbluth, A.W., Rosenbluth, M.N., Teller, A.H., Teller, E. Equation of state calculations by fast computing machines. *J. Chem. Phys.*, 21, 1087-1092 (1953).



Extended Data Figure 1 | Membership Selection. The spectroscopic dataset in the plane (v_{los}, R) , colour-coded according to the probability of each target belonging to the stellar population of And II. Non-member targets with velocities higher than the systematic velocity of And II ($v_{\text{sys}} = -191.4 \pm 0.4$) are foreground contaminants from the Milky Way, while non-member targets at lower negative velocities are interlopers from the Andromeda halo.



Extended Data Figure 2 | Velocity dispersion profile. And II displays an approximately flat velocity dispersion profile, except for a significant dip near the average projected radius of the stellar stream. Points of different sizes and color-depths refer to different circular annuli sizes (as in the legend), while error bars display 68% confidence levels.



Extended Data Figure 3 | Color Magnitude Diagram. The distribution of the stars belonging to the stream (blue points) and stars in the control sample (red points) in V-band magnitude versus V-I color.